Supporting Information

Synchronizing Carrier Extraction and Dielectric Coupling in a Hierarchical Homeometallic Plasmonic Catalyst for Light-Driven Nitrate Reduction

*Shuang Liu[a, #], Xinge Hu[a, #], Yuhan Xi[a], Qianyue Feng[a], Kaiqi Nie[b], Liu Cao[a], Yifei Xue[a], Chaoran Li[a], Kai Feng[a], Thongthai Witoon[c], Waleeporn Donphai[c], Jingjing Liu[d], Le He *[,a], and Xingda An*[,a]*

[a]Institute of Functional Nano & Soft Materials (FUNSOM) and Jiangsu Key Laboratory of Advanced Negative Carbon Technologies, Soochow University, Suzhou 215123, PR China.

[b]Department of Chemical Engineering, Tsinghua University, Beijing 100084, PR China.

[c]Center of Excellence on Advanced Adsorbents and Catalysts for Carbon Capture and Utilization, Department of Chemical Engineering, Faculty of Engineering, Kasetsart University, Bangkok 10900, Thailand.

[d]Institute of Information Technology, Suzhou Institute of Trade and Commerce, Suzhou 215009, PR China.

[#]These authors contributed equally to this work.

*Corresponding authors: Le He (lehe@suda.edu.cn), Xingda An (xdan@suda.edu.cn).

1. Experimental Section

Materials: All chemicals were used as received without further purification. Gold acid chloride trihydrate ($HAuCl_4 \cdot 3H_2O$, ⩾99.9%) was purchased from Shanghai Aladdin Biochemical Technology Co.,Ltd. L-Ascorbic acid (AA, 99.99%), polyvinylpyrrolidone (PVP, average mol wt 10000) were purchased from Macklin. Trisodium citrate dihydrate ($C_6H_5Na_3O_7 \cdot 2H_2O$) was purchased from Enox. Potassium Iodide (KI, 99%) was purchased from Sigma-Aldrich. Sodium borohydride ($NaBH_4$, 99%) was purchased from Thermo Scientific. Milli-Q water (Millipore, 18.2 MΩ cm at 25°C) was used in all experiments.

Preparation of large Au (Au_L) template NPs: Au nanoparticles (NPs) were synthesized through a modified seed-mediated growth approach as previously reported[1]. Seed solution was first prepared by mixing water solutions of $HAuCl_4$ (5 mM, 1 mL) and $C_6H_5Na_3O_7$ (1 mL, 5 mM), and diluting to a total volume of 18 mL DI water. Then, a reducing agent containing 10 mM $NaBH_4$ was added under vigorous stirring. The color of the seed solution turned dark brown after adding the reducing agent. For NPs growth, a growth solution containing aqueous solutions of PVP (1 wt%, 5 mL) and $HAuCl_4$ (0.25 M, 3.6 mL) was prepared. Then, the mixed solution containing 5 mL AA (0.1 M) and 5 mL KI (0.2 M) was added into the growth solution. Finally, 5 μL seed solution was added into the growth mixture with violent stirring for 20 minutes, then washed three times with deionized water, and stored at 4 ℃ for further use.

Preparation of $Au_{L\text{-}S}$ hierarchical homeometallic plasmonic catalyst: In the preparation of the $Au_{L\text{-}S}$ homometallic plasmonic catalyst, a photochemical deposition method was utilized. The reaction was carried out at room temperature, specifically, 100 μL of a 1 wt% PVP solution was added to 1 mL of the Au_L solution (934 ppm as determined by ICP-OES) and stirred thoroughly at 300 rpm, followed by the addition of 900 μL of 0.1 M $HAuCl_4$ precursor solution. The mixture was irradiated using a 620 nm monochromatic LED light source with an intensity of 350 mW/cm^2 for 10 minutes. Subsequently, the product was washed three times with deionized water (6000 rpm, 20

min) to remove any unreacted $HAuCl_4$. During the reaction, plasmonic hot electrons generated by the Au_L NPs facilitated the reduction of Au^{3+} into Au_S NPs on the surface of the Au_L NPs, leading to the formation of the Au_{L-S} hierarchical homometallic plasmonic catalyst.

Characterizations: Transmission electron microscopy (TEM) images and Energy-Dispersive X-Ray Spectroscopy (EDS) mappings were obtained with an FEI Talos F200X S/TEM at 200 kV. Fourier Transform Infrared Spectroscopy (FTIR) spectrum was obtained using a Fourier Transform Infrared Spectrometer (VERTEX70, Bruker). UV-vis absorbance spectra were obtained using a Lambda 750 UV/VIS/NIR spectrometer from PerkinElmer. The Raman analysis was conducted with the Renishaw InVia confocal Raman Microscope. Photoluminescence (PL) spectra were obtained using transient fluorescence spectroscopy (PL-TCSPC), the steady-state PL results were fitted with a Gaussian function. In situ XPS characterization (ISI-XPS) was collected on Thermo Escalab 250Xi photoelectron spectrometer equipped with nonmonochromatized Al-Kα X-ray with a photon energy of 1486.6 eV as the excitation source.

Photoelectrochemical (PEC) measurements: Linear Sweep Voltammetry (LSV) curves, amperometric i-t curves (Chronoamperometry, CA), electrochemical impedance spectroscopy (EIS) Nyquist plots and Mott-Schottky plots were measured on a CHI 660E electrochemical workstation (CH Instruments Ins.) in a three-electrode system: a 5 mm-diameter Glassy Carbon (GC) working electrode, a standard Ag/AgCl reference electrode and a platinum wire counter electrode. 15 μL of Au_{L-S} colloid was drop casted onto the GC electrode. All PEC tests were measured in an acid electrolyte with in an aqueous electrolyte containing 1 M KOH and 0.1 M $NaNO_3$. A scan rate of 50 mV/s and a collection frequency of 10 Hz were used. The potential of -0.8 V and 1 V with the similar collection rate of 1 Hz were adopted for the CA measurement in electrolyte. During the experimental process, LSV and amperometric i-t curves were obtained using full-spectrum Xe-lamp and LED with the nominal wavelength of 620 nm

(corresponding to the red edge of Au_L LSPR band) illumination with the light intensity of 100 mW/cm^2. The wavelength dependence test used monochromatic-light LEDs with wavelengths of 365, 420, 470, 520, 590, 620, 740 nm (MC-LED-M-λ, Beijing MerryChange Technology Co., Ltd.) with the light intensity of 100 mW/cm^2. The intensity-dependent photoelectrochemical test also used the full-spectrum Xe-lamp and 620 nm LED illumination by adjusting the light intensity of illumination from 100 to 400 mW/cm^2 and 50 to 300 mW/cm^2, respectively. EIS Nyquist plots were collected at an open circuit -1 V, with a frequency range from 1000 to 10 Hz.

Current density (mA/cm^2) was calculated from the measured current and the total geometric surface area (SA) of different samples on the working electrode[2]. For the particulate photocatalyst, the calculated geometric surface area gives a conservative estimation of the current densities and photocurrent densities. Photocurrent densities (J_{photo}, mA /cm^2) were calculated by subtracting the current densities in dark from those measured with illumination.

Fluorescence spectroscopy measurements: Fluorescence spectra were obtained with a transient fluorescence spectrometer (Edinburgh FLS1000). In the transient fluorescence measurements, the time-correlated single photon counting (TCSPC) technique was used, a 24-ps 375 nm laser as an excitation source was generated by an EPL laser, the signals were detected with an Edinburgh PMT detector, and fluorescence lifetimes were obtained by fitting the initial data with a biexponential decay function (ExpDec2). The instrument response function (IRF) of our setup is measured to be around 69 ps, as determined by biexponential decay fitting.

In-situ irradiated X-ray photoelectron spectroscopy (ISI-XPS) measurements: X-ray photoelectron spectroscopy was performed on XPS Thermo Escalab 250Xi. During the experimental process, full-spectrum light source with the light intensity of 100 mW/cm^2 (HF-GHX-XE-300) were used as the illumination source. The light irradiation was introduced into the analysis chamber through the quartz window, which allowed

illumination from the top. Then, the spectra of Au 4 f and Fe 2p were analyzed in dark and under light conditions to investigate the behavior of electron transfer.

Raman spectroscopy measurements: The in-text Raman spectra and maps of different samples were measured on drop-casted thin films of samples on silicon wafer substrates (⟨100⟩, Ferrotec Shanghai) or in an *in-situ* electrolysis cell with the Renishaw InVia confocal Raman Microscope with 100× air objective (Leica, Numerical Aperture = 1.25). Excitation laser of 532 nm (1800 l/mm diffraction grating), 633 nm (1800 l/mm diffraction grating), and 785 nm (1200 l/mm diffraction grating) were used with 0.5% laser powers and 10 s exposure time.

Theoretical Calculations: The finite-difference in time domain (FDTD) method, the core idea of which is to discretize the solution space into a rectangular mesh in Cartesian coordinates, is used to obtain the relationship between the electromagnetic field and the corresponding wavelengths by solving the complex geometrical Maxwell's system of equations as well as by performing the Fourier transform during the simulation. Here a TFSF (total-field scattering field) light source is used to simulate the electric field around $Au_{L\text{-}S}$ and controls. In the simulation, the diameter of the Au_L and Au_S NP were obtained from the TEM data, corresponding 120 nm and 6 nm, respectively. Meanwhile, the refractive index data of the Au and SiO_2 layer are derived from the models of Johnson and Christy and the Palik, respectively. Electric potential simulations were performed using the Electrostatics module in COMSOL Multiphysics on $Au_{L\text{-}S}$ and controls.

2. Supplemental Data Section

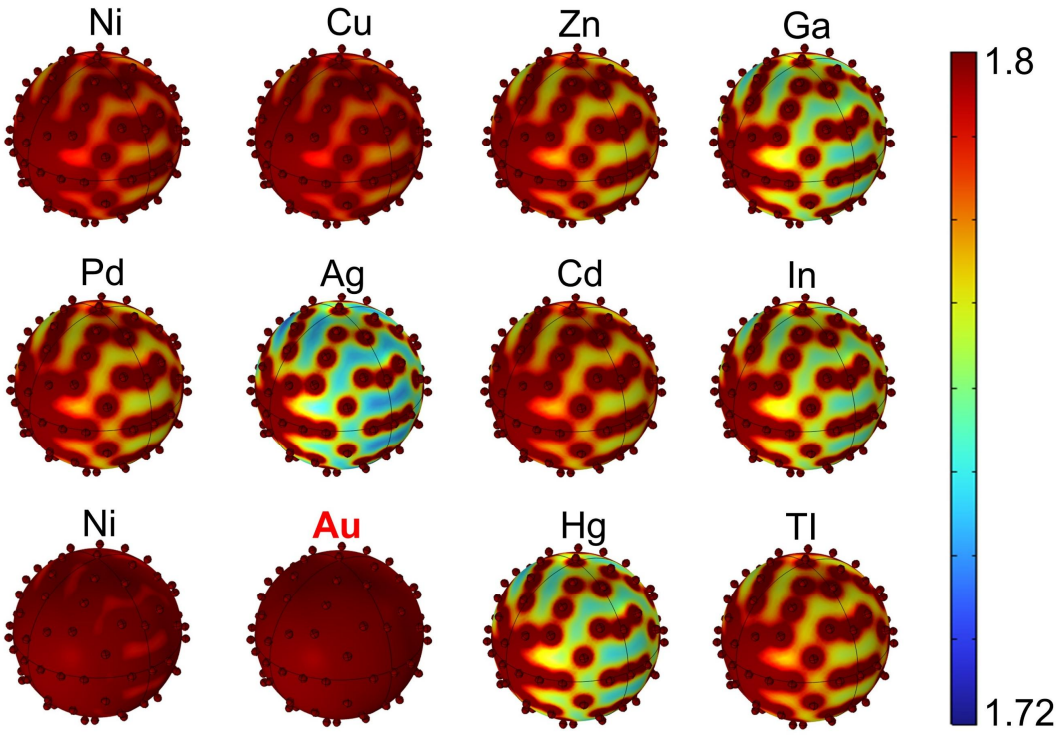

Figure S1. Theoretical simulation of the charge extraction efficiency using different reactor components.

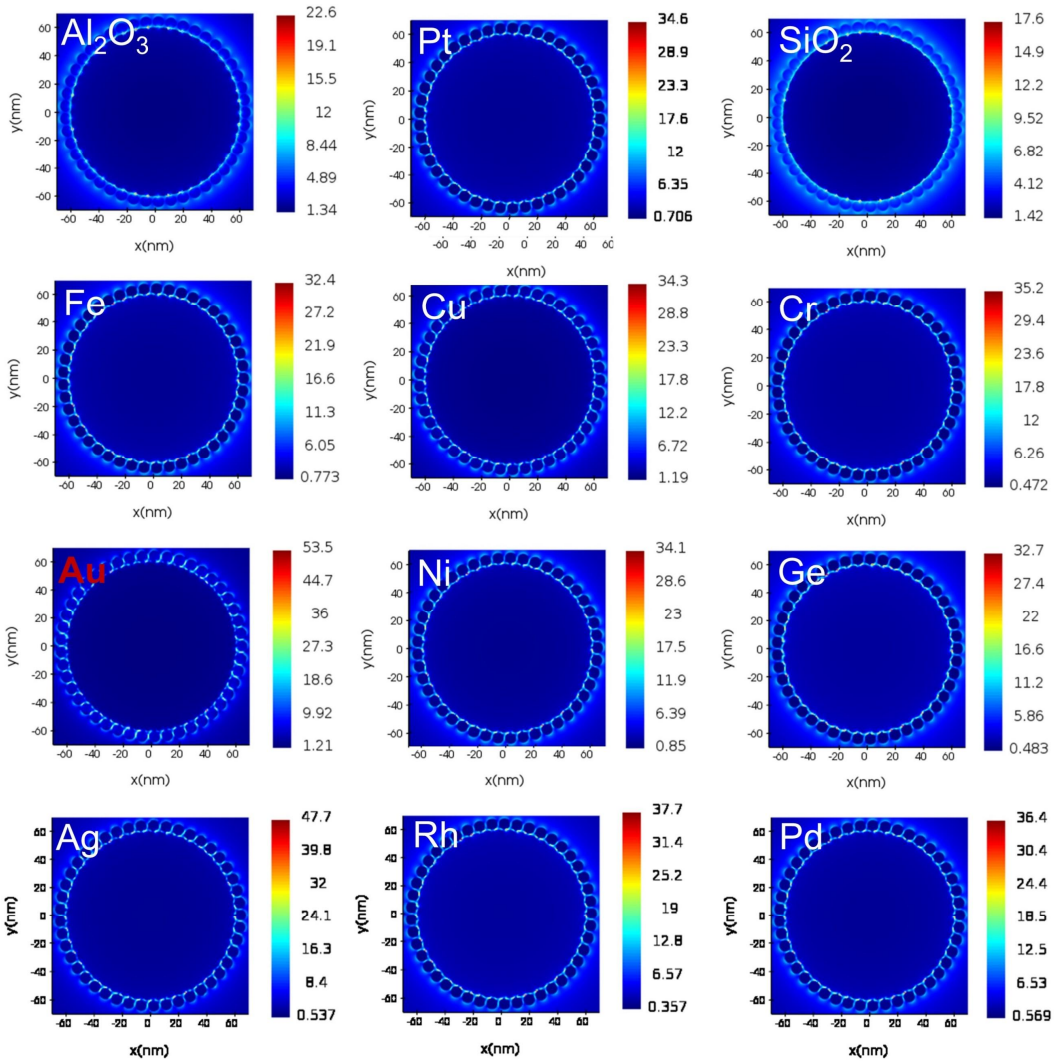

Figure S2. Field intensity maps with various reactor components corresponding to different dielectric constants in Fig. 1d. The dielectric constants (ε_r) of the above materials are: Al_2O_3 = 3.16; Pt = -8.99; SiO_2 = 2.14; Fe = -4.05; Cu = 4.997; Cr = -11.02; Au = -4.70; Ni = -7.09; Ge = 19.27; Ag = -11.54; Rh = -20.42; Pd = -8.99.

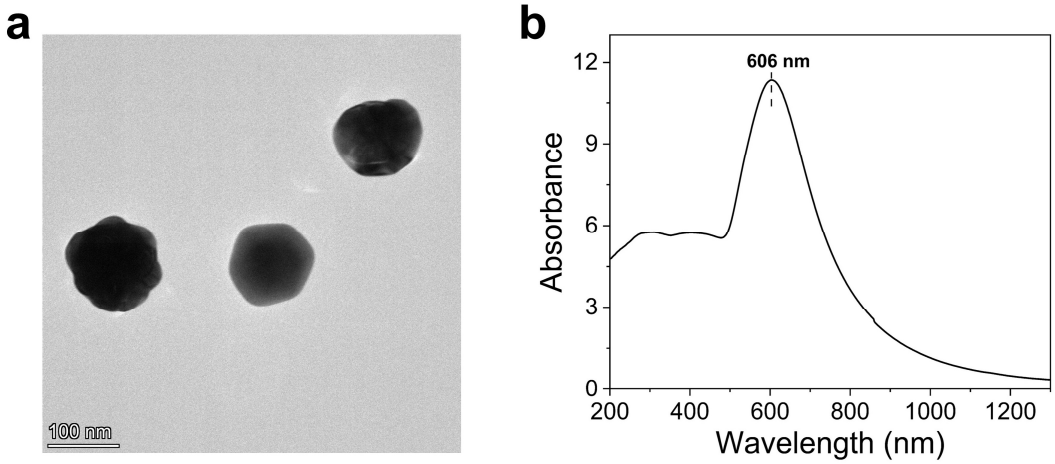

Figure S3. (a)TEM image and (b) UV-Vis-NIR absorbance spectra of Au_L template NPs.

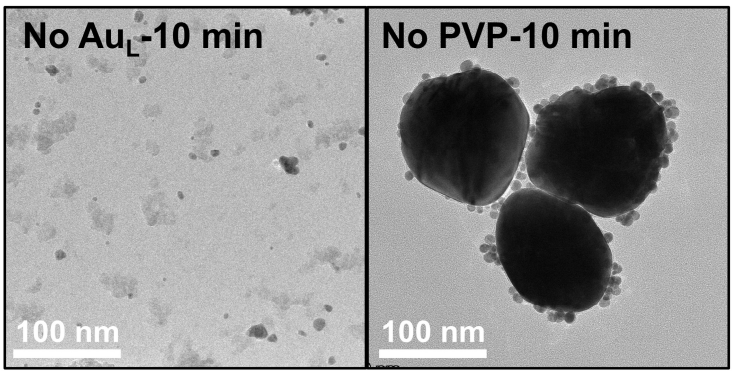

Figure S4. TEM images of photo-deposition products under different reaction conditions.

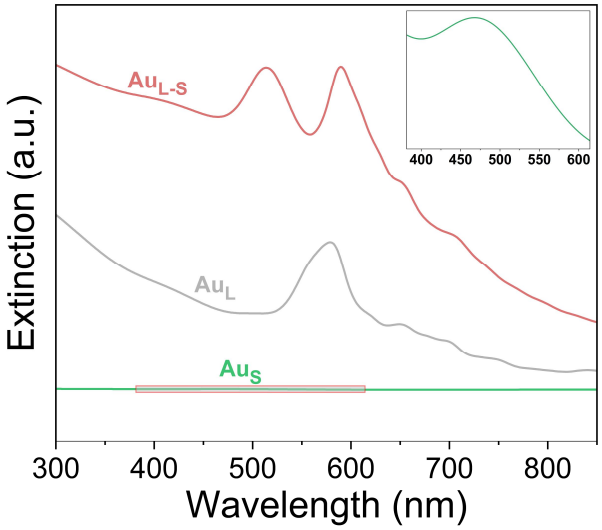

Figure S5. Extinction spectra of Au_{L-S}, Au_L and Au_S NPs.

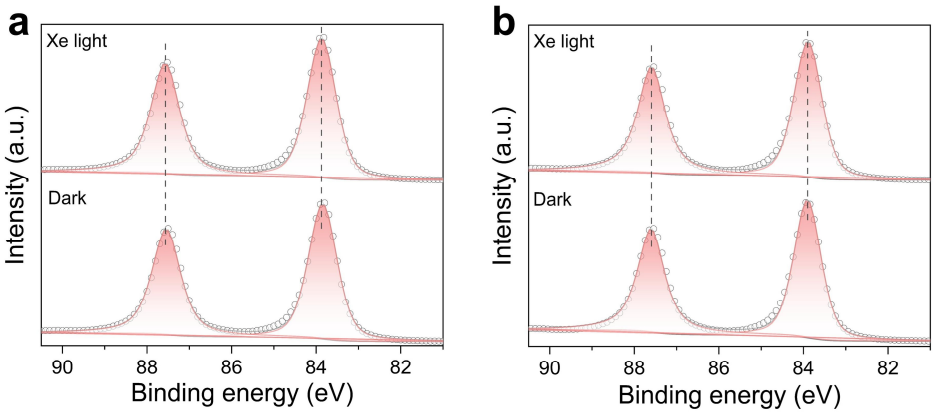

Figure S6. Au 4f XPS spectrum and fittings of (a) Au_L and (b) Au_S NPs.

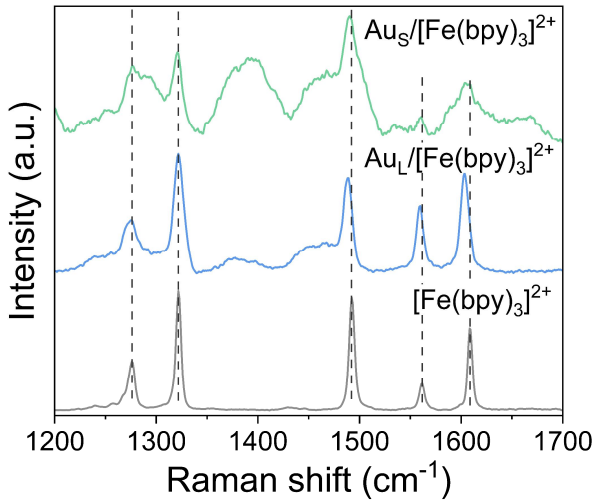

Figure S7. Raman spectra of $[Fe(bpy)_3]^{2+}$, $Au_L/[Fe(bpy)_3]^{2+}$ and $Au_S/[Fe(bpy)_3]^{2+}$.

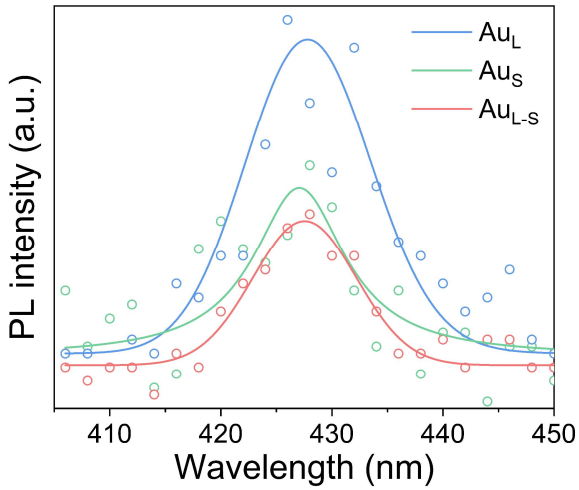

Figure S8. Steady-state PL spectra of $Au_{L\text{-}S}$ and controls of Au_L and Au_S.

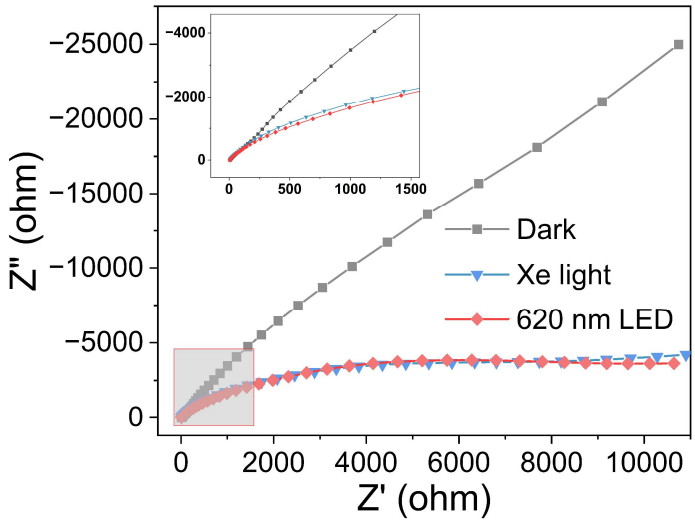

Figure S9. EIS Nyquist plots of $Au_{L\text{-}S}$ in dark or under irradiation with the intensity of 100 mW/cm^2.

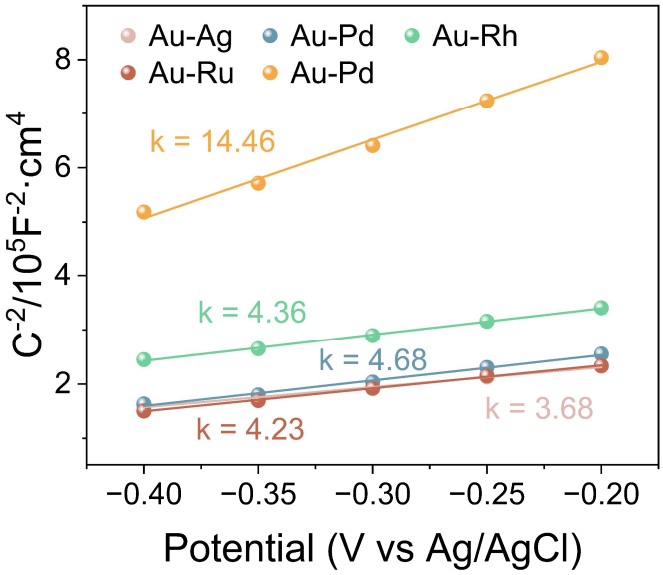

Figure S10. Mott-Schottky plots of various heterobimetallic catalysts under Xe light irradiation.

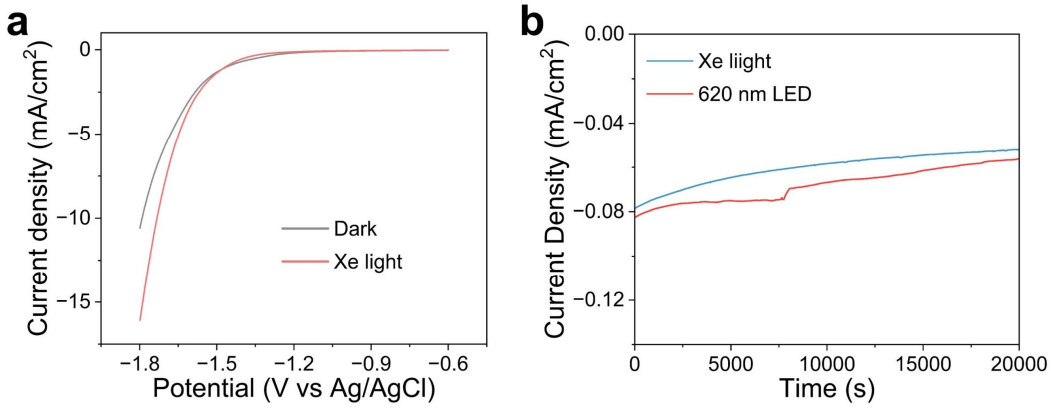

Figure S11. (a) Photoelectrochemical LSV curves for standalone Au NPs only and (b) Chronoamperometric I-t curves at −1 V (vs Ag/AgCl) for $Au_{L\text{-}S}$ in dark or under irradiation with the intensity of 100 mW/cm^2.

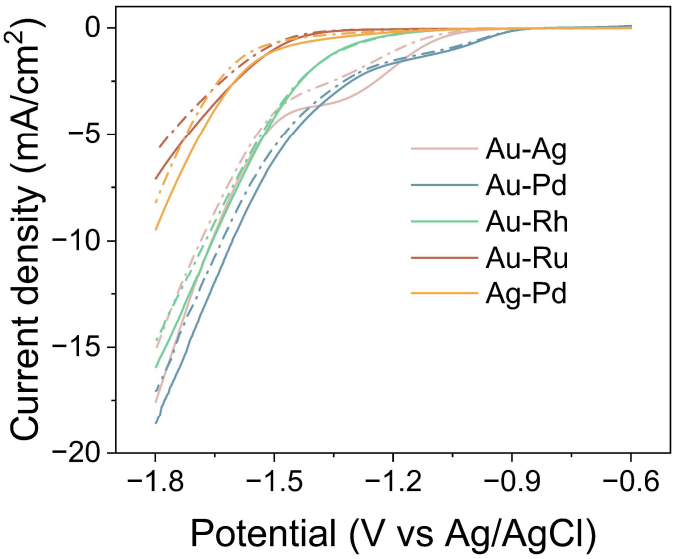

Figure S12. LSV curves of various heterobimetallic catalysts. The solid and dashed lines represent data obtained under irradiation and in dark, respectively.

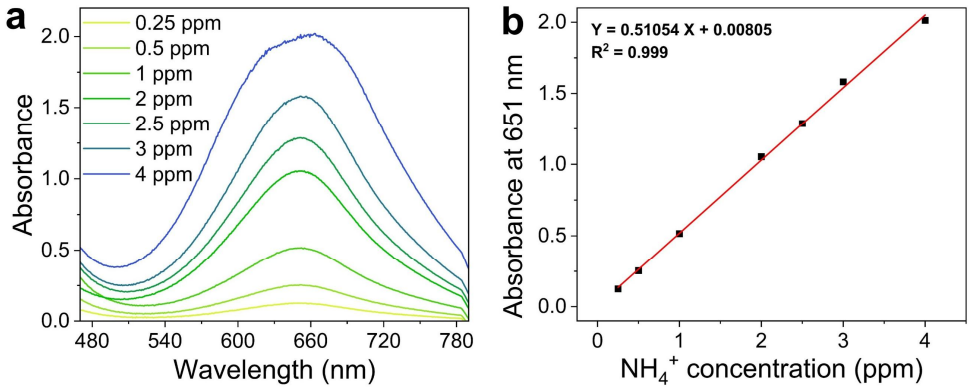

Figure S13. (a) UV-Vis-NIR curves and (b) calibration curve for calibration samples of known concentrations used in the indophenol blue staining experiment for ammonia product quantification.

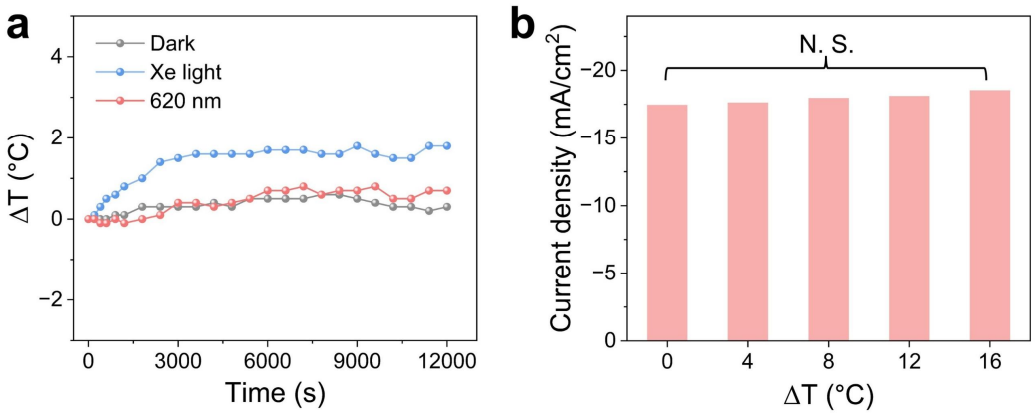

Figure S14. (a) Temperature changes of electrolyte in NO_3RR process in dark or under irradiation measured by thermocouples. (b) Histograms of current densities corresponding to $Au_{L\text{-}S}$ catalyzed NO_3RR at temperatures up to 16 °C higher than room temperature.

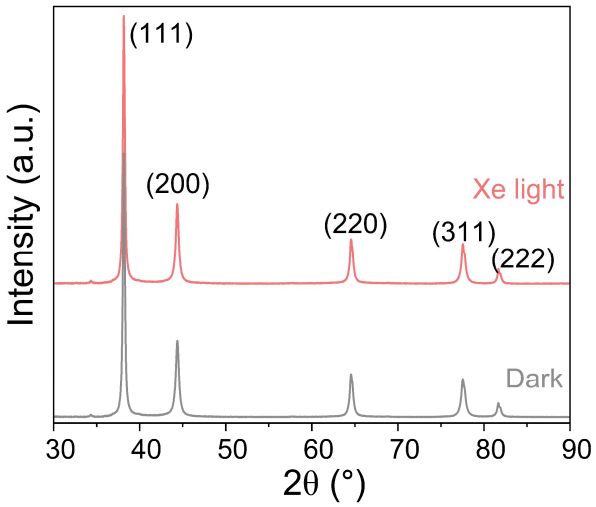

Figure S15. XRD pattern of $Au_{L\text{-}S}$ in dark or under irradiation with the intensity of 100 mW/cm^2.

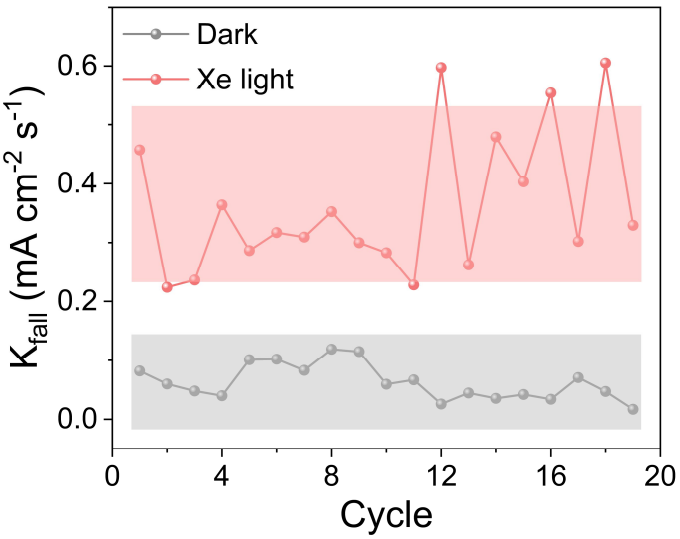

Figure S16. Changes of the slope in the rising part (k_{rise}).

Supporting References

1. J. Feng, D. Xu, F. Yang, J. Chen, C. Wu and Y. Yin, *Angew. Chem. Int. Ed.*, 2021, **60**, 16958-16964.
2. S. Liu, Z. Wu, Z. Zhu, K. Feng, Y. Zhou, X. Hu, X. Huang, B. Zhang, X. Dong, Y. Ma, K. Nie, J. Shen, Z. Wang, J. He, J. Wang, Y. Ji, B. Yan, Q. Zhang, A. Genest, X. Zhang, C. Li, B. Wu, X. An, G. Rupprechter and L. He, *Nat. Commun.*, 2025, **16**, 2245.